Inorganic Chemistry

pubs.acs.org/IC

Article

Two-Electron Redox Tuning of Cyclopentadienyl Cobalt Complexes Enabled by the Phenylenediamide Ligand

Minzhu Zou, Thomas J. Emge, and Kate M. Waldie*

Cite This: *Inorg. Chem.* 2023, 62, 10397−10407

Read Online

ACCESS | Metrics & More | Article Recommendations | Supporting Information

ABSTRACT: Achieving multielectron activity at first-row transition-metal complexes has important implications for homogeneous catalysis using earth-abundant metals. Here, we report a family of cobalt−phenylenediamide complexes that undergo reversible 2e$^-$ oxidation regardless of the ligand substituents, enabling unprecedented multielectron redox tuning over 0.5 V and, in each case, affording the dicationic Co(III)-benzoquinonediimine species. The neutral complexes are best described as delocalized systems with π-bonding in the metallocycle, consistent with a closed-shell singlet ground state predicted by density functional theory (DFT) calculations. Our DFT results also predict an ECE pathway for 2e$^-$ oxidation (ECE = electrochemical step, chemical step, electrochemical step), where the first 1e$^-$ step involves redox-induced electron transfer to yield a Co(II) intermediate. Disruption of the metallocycle bonding in this state enables a change in the coordination geometry through association of an addition ligand, which is critical for accessing the potential inversion. The electronic properties of the phenylenediamide ligand govern whether the second electron is lost from the ligand or metal, providing a remarkable example of tunable 2e$^-$ behavior at first-row systems.

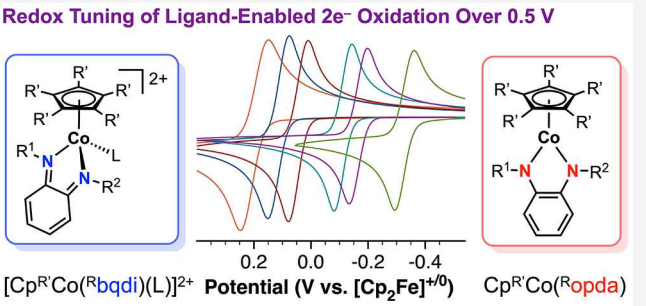

INTRODUCTION

The transfer of multiple electrons through redox processes is central to many chemical, electrochemical, and biological transformations. While prevalent at late second- and third-row transition-metal complexes, 2e$^-$ redox couples are rare at mononuclear first-row transition-metal systems, which instead favor sequential 1e$^-$ transfer events at well-separated potentials due to the high electrostatic penalty associated with the second transfer. This behavior poses a fundamental challenge, often resulting in 1e$^-$ radical-based reactivity or larger overpotentials for electrocatalytic reactions with the more earth-abundant 3d metals.[1,2] An overall 2e$^-$ redox process can be accomplished when the second electron transfer is more energetically favorable than the first, a situation known as potential inversion.[3] Developing first-row transition-metal complexes that can mediate multielectron processes and thus mimic noble metal reactivity continues to be of great interest.[4−7]

Redox-active ligands have emerged as a strategy for accessing greater redox flexibility and multielectron behavior at first-row metal complexes due to their ability to serve as electron reservoirs.[8−12] The design of many redox-active ligands is inspired by metalloenzymes, which often facilitate multielectron transformations through the cooperative effects of transition-metal cations and redox cofactors. However, introduction of redox-active ligands into a transition-metal complex does not guarantee that 2e$^-$ processes will be favored over 1e$^-$ reactivity.[2] In fact, only a handful of mononuclear first-row metal complexes with redox-active ligands exhibit a 2e$^-$ redox couple,[13−26] often accompanied by ligand coordination or dissociation that promotes potential inversion. Among these limited first-row metal examples, 2e$^-$ reduction processes have been studied more extensively; the few examples of quasi-reversible 2e$^-$ oxidation behavior were not explored in detail.[23−26]

A classic redox-active ligand is *o*-phenylenediamide (opda), which has three accessible oxidation states when bound to a metal center: opda^{2-}, semibenzoquinonediimine (s-bqdi$^{\cdot-}$), and benzoquinonediimine (bqdi^0) (Scheme 1a). Many seminal studies have examined the electronic structure and reactivity of numerous metal−opda complexes[24−31] and related diazabutadiene systems.[32,33] With cobalt, the lower energy of the metal d orbitals enables effective matching with the opda π system, giving rise to strong orbital mixing.[28] In some cases, these properties have been exploited to promote overall 2e$^-$ transformations with organic substrates at cobalt, where the

Received: April 20, 2023
Published: June 21, 2023

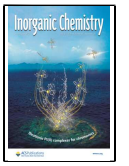

https://doi.org/10.1021/acs.inorgchem.3c01283
Inorg. Chem. 2023, 62, 10397−10407

Scheme 1. (a) Ligand-Centered Redox Series of Metal−opda Complexes; (b) Possible Electronic Structures of CpCo(opda) (1); (c) Reversible 2e⁻ Oxidation of [Cp$^{R'}$Co(^{R}opda)] (R′ = H or Me; R^1, R^2 = H, Ureayl, or Isopropyl)

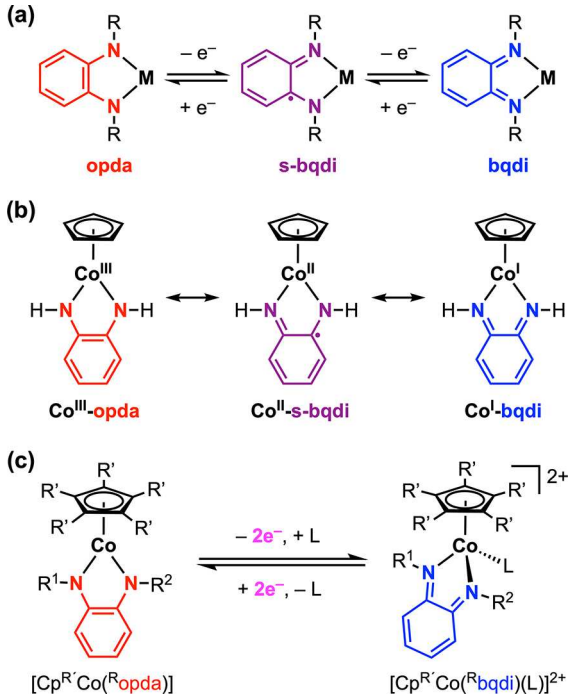

opda (or related) ligands may be viewed as an electron reservoir.[34,35]

While many reports have focused on homoleptic systems, half-sandwich complexes [Cp$^{R'}$M(^{R}opda)] (Cp^{H} = cyclopentadienyl; Cp^{Me} = Cp* = pentamethylcyclopentadienyl) have been shown to possess unique electrochemical properties that depend on the ligand identity and nature of the metal center. For [Cp*Ir] complexes containing an amidophenolate or diphenyl-opda ligand, two distinct 1e⁻ oxidation waves are observed by cyclic voltammetry (CV), while the monophenyl-opda analogue exhibits a 2e⁻ oxidation at slower scan rates.[36−38] In each case, the iridium complexes were formally assigned as Ir^{III} with a dianionic opda (or related) ligand, thus the oxidation processes are thought to be ligand-based. Recently, Sarkar and co-workers reported a series of [Cp*Rh] complexes where the CV behavior varies with the opda substituents: electron-poor sulfonyl derivatives showed 1e⁻ waves, while the electron-rich phenyl versions undergo a 2e⁻ oxidation.[39] Such rhodium systems are assigned as coordinatively unsaturated species with a formal Rh^{III} center.[39−41] In contrast, over the past four decades, discussions on CpCo(opda) (**1**) and related [CpCo] or [Cp*Co] systems have been dominated by the Co^{I}-bqdi assignment (Scheme 1b),[42−46] despite structural similarities to other M−s-bqdi and M−opda systems. Additionally, recent electrochemical studies showed that **1** and a perfluoro analogue can be reversibly oxidized at mild potentials, but this oxidation was erroneously assigned as a 1e⁻ process.[45,46] The lack of detailed analysis of this oxidation process motivated our further study into this family, with the aim to better illuminate the electronic structure and electrochemical behavior of these cobalt complexes.

Herein, we report a series of [Cp$^{R'}$Co(^{R}opda)] complexes **1**−**5** and unequivocally show that these complexes all undergo a reversible 2e⁻ oxidation, affording a notable new example of potential inversion and multielectron activity, in particular multielectron oxidation, at first-row transition-metal complexes. This reversible redox behavior is maintained across the full series, for the first time, demonstrating redox tuning of a 2e⁻ oxidation feature at first-row transition-metal complexes as a function of ligand properties. Independent synthesis and characterization of the doubly oxidized complexes confirm that 2e⁻ oxidation generates Co^{III}−bqdi systems (Scheme 1c). Experimental and computational analyses indicate covalent π-bonding in the neutral complexes and reveal trends in the sites of electron transfer. The structural changes that accompany 2e⁻ oxidation point to the active involvement of the redox-active ligand in this process.

RESULTS AND DISCUSSION

Synthesis. The substituted phenylenediamine ligands (^{R}opdaH$_2$) were prepared by the reaction of *o*-phenylenediamine with isocyanate (for R = ureayl) or 2-iodopropane (for R = isopropyl).[47−49] The synthesis of **1**−**5** was performed by initial deprotonation of ^{R}opdaH$_2$ with 2 equiv base in anhydrous THF, followed by salt metathesis with CpCo(CO)I$_2$ or Cp*Co(CO)I$_2$ (Scheme 2). Alternate syntheses of **1** and

Scheme 2. Synthesis of Neutral and Dicationic Cobalt Complexes

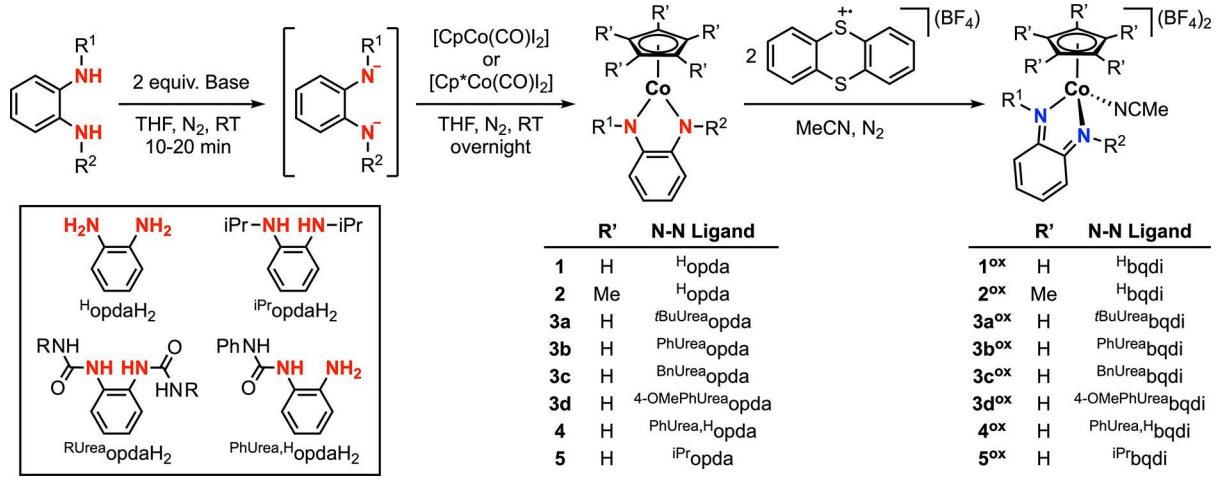

	R′	N-N Ligand
1	H	^{H}opda
2	Me	^{H}opda
3a	H	$^{t\text{BuUrea}}$opda
3b	H	$^{\text{PhUrea}}$opda
3c	H	$^{\text{BnUrea}}$opda
3d	H	$^{\text{4-OMePhUrea}}$opda
4	H	$^{\text{PhUrea,H}}$opda
5	H	$^{i\text{Pr}}$opda

	R′	N-N Ligand
1^{ox}	H	^{H}bqdi
2^{ox}	Me	^{H}bqdi
3a^{ox}	H	$^{t\text{BuUrea}}$bqdi
3b^{ox}	H	$^{\text{PhUrea}}$bqdi
3c^{ox}	H	$^{\text{BnUrea}}$bqdi
3d^{ox}	H	$^{\text{4-OMePhUrea}}$bqdi
4^{ox}	H	$^{\text{PhUrea,H}}$bqdi
5^{ox}	H	$^{i\text{Pr}}$bqdi

https://doi.org/10.1021/acs.inorgchem.3c01283
Inorg. Chem. 2023, 62, 10397−10407

2 have been reported using aqueous sodium hydroxide.[50,51] Complexes **1**−**5** are diamagnetic and air-stable. They display well-resolved, sharp signals by ^{1}H NMR, in agreement with previous reports on **1** and **2**.[50,51] Variable temperature NMR spectra for **3a** show no signal broadening up to 45 °C (Figure S24), and magnetic susceptibility measurements using the Evans method are consistent with a singlet ground-state. The isopropyl C−H in **5** is a broad signal at 25 °C due to the rotation of the isopropyl groups in solution. Different conformations of **5** with respect to the isopropyl group orientations become distinguishable at lower temperatures (Figure S37).

Treatment of the neutral complexes with 2 equiv chemical oxidant in acetonitrile yields the doubly oxidized dicationic complexes $[Cp^{R'}Co(^{R}bqdi)\ (MeCN)]X_2$ (R′ = H or Me, X = PF_6^- or BF_4^-) in high yield (Scheme 2). While $AgPF_6$ may be used as the chemical oxidant, thianthrenium tetrafluoroborate ($(Thi^{+})BF_4$, $E_{1/2}$ = 0.86 V vs $[Cp_2Fe]^{+/0}$)[52] resulted in cleaner reactivity with less decomposition (see Supporting Information). Chemical oxidation to obtain $\mathbf{2^{ox}}$ and $\mathbf{5^{ox}}$ can be performed at 25 °C, while $\mathbf{1^{ox}}$, $\mathbf{3a^{ox}}$−$\mathbf{3d^{ox}}$, and $\mathbf{4^{ox}}$ require low-temperature synthesis. The oxidized complexes are all diamagnetic species. The ^{1}H NMR spectrum of $\mathbf{2^{ox}}$ shows the NH resonance at 11.80 ppm (Figure S42), consistent with the diimine form in the bqdi ligand.[53] Given that the chemical shift of the NH signal in **2** is significantly more upfield (8.37 ppm), it appears reasonable to discount the Co^{I}−bqdi description for the neutral complexes (Scheme 1b). ^{1}H NMR analysis also reveals the different solution-phase stability of the oxidized complexes: $\mathbf{3a^{ox}}$−$\mathbf{3d^{ox}}$ and $\mathbf{4^{ox}}$ are stable in CD_3CN at −20 °C but slowly decompose to $[CpCo(MeCN)_3]^{2+}$ and unidentified species over 16 h at 0 °C (Figure S47); solutions of $\mathbf{1^{ox}}$ and $\mathbf{2^{ox}}$ in CD_3CN are stable for at least 5 h at 4 °C (Figures S39 and S44); no changes are observed by ^{1}H NMR when a solution of $\mathbf{5^{ox}}$ in CD_3CN is exposed to air for 28 h at 25 °C (Figure S61).

X-ray Crystallography. The crystal structures of **3a**−**3d**, **4**, and **5** show a two-legged piano stool, half-sandwich geometry, where the Cp ligand is nearly perpendicular to the Co−phenylenediamide plane (see Figure 1a and Supporting Information). The phenylene backbone shows a small degree of C−C bond length alternation between 1.40−1.43 Å and 1.35−1.38 Å, indicating some loss of aromaticity compared to $opdaH_2$. These results are consistent with the structures of **1** and **2**.[42,44] The average Co−N and $N-C_{phenylene}$ bond lengths are 1.86 ± 0.02 and 1.37 ± 0.01 Å, respectively, which are shorter than typical Co−N and N−C single bonds and suggest the presence of π-conjugation across the Co−opda metallocycle.[24,26,27] In contrast, the $N-C_{phenylene}$ bond lengths in $^{t\mathrm{BuUrea}}opdaH_2$ are 1.442(11) Å, ca. 0.07 Å longer than the corresponding bonds in **3a**. The structure of **5** shows different orientations of the isopropyl groups in the crystal lattice. While the trans orientation was found here, both the trans and syn geometries are accessible in solution, as observed by ^{1}H NMR (vide supra).

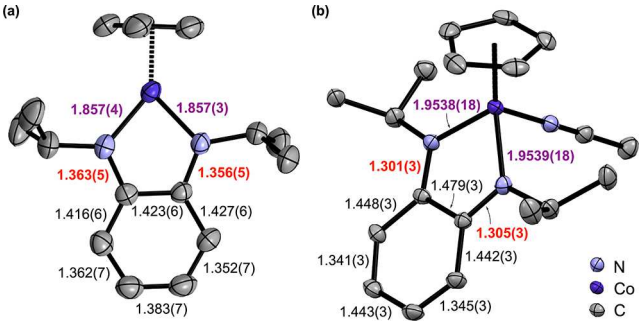

Figure 1. Structure of (a) **5** and (b) $\mathbf{5^{ox}}$ with selected bond lengths (Å). Hydrogen atoms, cocrystallized solvent, and BF_4^- counterions omitted for clarity. Ellipsoids shown at 50% probability.

While we could not obtain crystals of $\mathbf{3a^{ox}}$−$\mathbf{3d^{ox}}$ and $\mathbf{4^{ox}}$ due to facile ligand loss in solution, single crystals of $\mathbf{1^{ox}}$, $\mathbf{2^{ox}}$, and $\mathbf{5^{ox}}$ were obtained at −35 °C (see Supporting Information). Compared to their neutral analogues, the dicationic complexes have a higher coordination number with an acetonitrile ligand. There is clear elongation of the Co−N bond lengths upon oxidation (0.1 Å longer), and the average $N-C_{phenylene}$ bond lengths in the oxidized complexes are shorter (1.30 ± 0.01 Å; Tables S28−S30). Also, the phenylene backbone shows a nonaromatic quinone structure with alternating single (ca. 1.44 Å) and double (ca. 1.34 Å) bonds. These structural metrics are typical of metal-diimine systems and indicate the $[Cp^{R'}Co^{III}(^{R}bqdi)\ (MeCN)]^{2+}$ formulation for the oxidized complexes.[54] This assignment is consistent with the diamagnetic ^{1}H NMR spectra of these species, being a coordinatively saturated low-spin Co^{III} center in a pseudo-octahedral geometry. The bqdi ligand is a weaker σ-donor than s-bqdi or opda, which likely contributes to the ligand loss observed for the oxidized complexes under certain conditions.

The doubly oxidized, dicationic complexes are thus unambiguously assigned as Co^{III}-bqdi systems. Turning to complexes **1**−**5**, we highlight the significant structural differences between the neutral and dicationic complexes. In particular, the substantial decrease in $N-C_{phenylene}$ bond lengths and the notable decrease in phenylene aromaticity upon oxidation indicate some degree of ligand involvement in the $2e^-$ oxidation. Thus, we conclude that the previous Co^{I}−bqdi assignment for complex **1** from Rheingold and co-workers is inappropriate (Scheme 1b).[42] At the same time, the solid-state structures of **1**−**5** are also not consistent with a formal Co^{III}−opda assignment, in which the $N-C_{phenylene}$ bond lengths are typically ca. 1.40 Å and the phenylene C−C bond lengths are identical.[24,27,28] Instead, the intermediate $N-C_{phenylene}$ bond lengths and other bond metrics in **1**−**5** suggest partial oxidation of the ligand, either as the semiquinone-type radical anion (s-bqdi) that is strongly antiferromagnetically coupled to a low-spin Co^{II} center or as the dianionic opda ligand with covalent π-bonding and delocalization across the Co^{III} metallocycle (Scheme 1b). These two possibilities are explored below using computational methods (vide infra).

Electrochemistry. Cyclic voltammetry (CV) studies of **1**−**5** display one reversible oxidation and one reversible reduction in 0.1 M $[^nBu_4N][PF_6]$ in MeCN (Table 1 and Figure 2). Notably, the peak-to-peak separation (ΔE_p) for oxidation of **1** and **2** is only 46 and 31 mV at 25 mV/s, respectively, while ΔE_p is 75 mV for the reduction of **1** at the same scan rate (Figures S66 and S67). The oxidation peak current is 2.4−2.7 times higher than that of the reduction for all complexes. These observations are consistent with a $2e^-$ oxidation and $1e^-$ reduction.[55] The reversibility of the $2e^-$ wave is maintained over a range of scan rates, and no evidence of discrete $1e^-$ events is observed, indicative of favorable potential inversion (see Supporting Information). Consistent with this assignment, $\mathbf{5^{ox}}$ shows a $2e^-$ reduction at the same potential as the

https://doi.org/10.1021/acs.inorgchem.3c01283
Inorg. Chem. 2023, 62, 10397−10407

Table 1. Cyclic Voltammetry Data of Complexes 1−5 and 5^{ox}[a]

complex	$E_{1/2}$ (V)[b]	ΔE_p (mV)[c]	i_c/i_a[d]	$E_{1/2}$ (V)[b]	ΔE_p (mV)[c]	i_c/i_a[d]
1	−0.11	53	0.94	−1.83	72	1.05
2	−0.33	58	0.95	−2.04	75	1.06
3a	0.11	61	1.01	−1.24	69	1.02
3b[e]	0.20	63	0.88	−1.03	67	1.16
3c[e]	0.15	53	0.94	−1.18	67	1.06
3d[e]	0.18	62	0.86	−1.09	65	1.04
4	0.044	61	0.92	−1.35	71	1.12
5	−0.17	63	0.98	−1.87	73	1.28
$\mathbf{5}^{ox}$[f]	−0.17	55	1.08	−1.88	80	1.21

[a]1 mM [Co], 0.1 M [^{n}Bu$_4$N][PF$_6$], MeCN, glassy carbon working electrode, Pt counter electrode, Ag/AgNO$_3$ reference electrode, 50 mV/s. [b]$E_{1/2} = (E_{p,a} + E_{p,c})/2$, $E_{p,a}$ and $E_{p,c}$ are anodic and cathodic peak potentials, respectively. Potentials vs $[Cp_2Fe]^{+/0}$. [c]$\Delta E_p = E_{p,a} - E_{p,c}$. [d]$i_{p,a}$ = anodic peak current, $i_{p,c}$ = cathodic peak current. [e]Solvent = MeCN/THF (4:1). [f]0.5 mM [Co], 100 mV/s.

2e$^-$ oxidation of **5** (Figures S88 and S89). This behavior also aligns with our results using chemical oxidants: two equivalents of oxidant are required for complete conversion to the doubly oxidized species, but treatment with fewer equivalents does not lead to a 1e$^-$ oxidized intermediate. Overall, the previous assignment for the oxidation of **1** and its fluorinated analogue as a 1e$^-$ process is inappropriate.[46] This 2e$^-$ behavior is in stark contrast to the electrochemistry of many square planar or tetrahedral cobalt complexes with opda-type ligands, which exhibit separate 1e$^-$ processes.[22,24,26,35,56] This novel but previously overlooked multielectron behavior motivated our further investigation into these complexes.

The ureayl derivatives **3a**−**3d** and **4** exhibit the most positive redox potentials in this series. Varying the substituents on the ureayl arms has limited effect on the 2e$^-$ oxidation potential, but changing the number of ureayl groups shifts the oxidation by ca. 150 mV per substituent (see Table 1). Introduction of electron-donating isopropyl groups in **5** shifts both redox couples more negative due to increased electron density in this complex. The electron-rich Cp* ligand in **2** has an even more significant impact on redox potentials, which are both shifted negative by ca. 200 mV compared to **1**, the Cp analogue. It is well known that the redox potentials of metal complexes are influenced by the electronic properties of the ligands. However, this series is a remarkable demonstration where the oxidation potential can be tuned by more than 0.5 V while maintaining reversible 2e$^-$ behavior.

Remarkably, the 2e$^-$ oxidation remains reversible in THF, CH_2Cl_2, or fluorobenzene with [^{n}Bu$_4$N][PF$_6$] (see Supporting Information), demonstrating that the potential inversion is still favorable with weakly coordinating solvents and/or supporting electrolyte ions. The 2e$^-$ oxidation feature of **3b** in MeCN with 0.05 M [^{n}Bu$_4$N][BArF$_{24}$] (BArF$_{24}^-$ = tetrakis[3,5-bis-(trifluoromethyl)phenyl]borate) shows partial loss of reversibility at slow scan rates ($i_{p,c}/i_{p,a}$ = 0.60 at 100 mV/s), but gradual addition of [^{n}Bu$_4$N][PF$_6$] increases reversibility (Table S21 and Figure S83). No evidence of sequential one-electron processes is observed. Surprisingly, the oxidation of **2** is still reversible in 0.05 M [^{n}Bu$_4$N][BArF$_{24}$] in MeCN or at faster scan rates in CH_2Cl_2 (Figures S74 and S75), and thus the reversibility of this feature appears to depend on the ligand identity and solution conditions. The large, noncoordinating BArF$_{24}^-$ anion may be unable to provide sufficient ion-pairing stabilization to the sterically bulky oxidized complexes such as $\mathbf{3b}^{ox}$, which may lead to partial decomposition of the dication in MeCN on the CV time scale and the poor reversibility of the oxidation feature. The ion-pairing strength of PF$_6^-$ is greater than that of the BArF$_{24}^-$ anion,[57] and thus the former likely stabilizes $\mathbf{3b}^{ox}$ enough to observe reversible behavior. In light of these CV results, we examined the oxidation of **5** with 2 equiv $AgPF_6$ in CH_2Cl_2. This reaction leads to the immediate formation of a brown precipitate, tentatively assigned as a doubly oxidized species stabilized by the hexafluorophosphate anion. The ^{1}H NMR analysis of this solid in CD_3CN is consistent with $[\mathbf{5}\text{-}\mathbf{CD_3CN}]^{2+}$, where the solvent is coordinated to the metal, and the ^{19}F NMR spectrum shows new resonances that suggest the active role of the PF$_6^-$ anion in the oxidation (Figures S62 and S63).

UV−Vis Spectroscopy. In line with the intense colors of **1**−**5**, the electronic spectra show a dominant transition in the

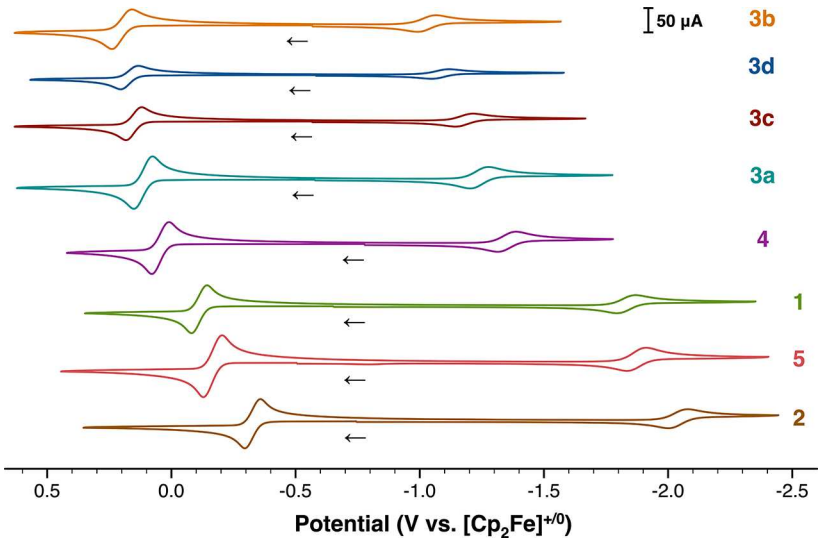

Figure 2. CVs of cobalt complexes in MeCN (**1**, **2**, **3a**, **4**, and **5**) or MeCN/THF (4:1; **3b**, **3c**, and **3d**) (1 mM [Co] and 0.1 M [^{n}Bu$_4$N][PF$_6$]; scan rate 100 mV/s).

https://doi.org/10.1021/acs.inorgchem.3c01283
Inorg. Chem. 2023, 62, 10397−10407

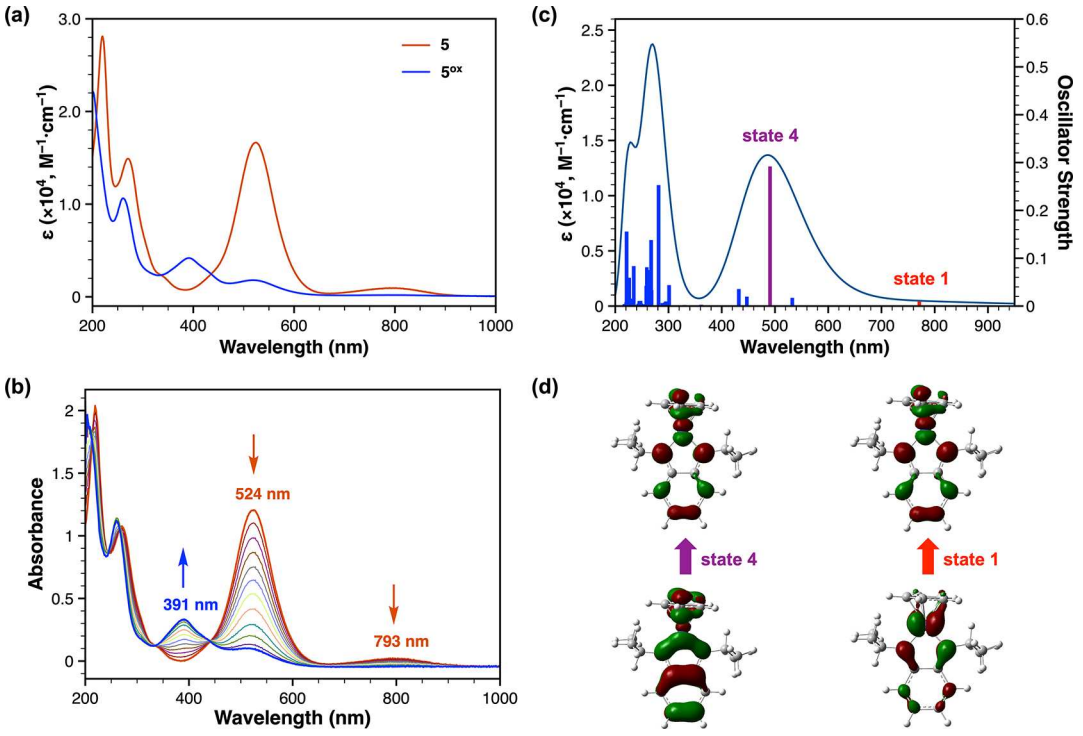

Figure 3. (a) Electronic absorption spectrum of **5** and $\mathbf{5}^{ox}$ in MeCN. (b) UV−vis SEC oxidation of **5** in MeCN. See Supporting Information for details. (c) Calculated electronic spectrum of **5** based on the TD-DFT wavelengths and oscillator strengths using Gaussian functions of hwhm = 2686 cm^{-1} (hwhm: half width at half-maximum). (d) Representative natural transition orbitals (isovalue = 0.04) of **5** for selected electronic transitions.

visible region at ca. 520−580 nm with molar absorption coefficients on the order of 20,000 $M^{-1}\cdot cm^{-1}$ (Figures 3a and S90−S98). The presence of ureayl substituents causes a red-shift of this absorbance for **3a**−**3d** and **4** compared to **1**. A weak absorption is also observed in the NIR region between 700 and 800 nm.

Time-dependent density functional theory (TD-DFT) calculations and natural transition orbital (NTO) analysis were used to clarify the main molecular orbital contributions to these electronic transitions (see Supporting Information). The calculated transitions for **5** (Figure 3c) and the other neutral complexes (Figures S120−S122) provide a reasonable match with the main features of the experimental spectrum. The intense visible absorption is mainly attributed to the HOMO−1 → LUMO transition, which has significant $\pi \rightarrow \pi^*$ character across the Co−N bonds (Figure 3d). The weak NIR absorption corresponds to the approximate HOMO → LUMO transition, where the HOMO has cobalt d_{xy} and phenylenediamide π characters. Similar assignments are obtained for the other neutral complexes (Tables S36−S38).

Upon oxidation, the visible absorption profile of $\mathbf{5}^{ox}$ is significantly decreased with weak transitions at 518 nm (ε = 1800 $M^{-1}\cdot cm^{-1}$) and 391 nm (ε = 4200 $M^{-1}\cdot cm^{-1}$), as seen in Figure 3a (blue trace). While $\mathbf{5}^{ox}$ shows good stability in solution at 25 °C, the solution stability of the other oxidized complexes is limited. However, we found these species to be sufficiently stable to be investigated on the spectroelectrochemistry (SEC) time scale, and thus UV−vis SEC studies were employed to probe in situ the $2e^-$ oxidation. Monitoring the oxidation of **5** shows a decrease of the characteristic bands at 524 and 793 nm with the appearance of a new band at 391 nm (Figure 3b), consistent with the formation of $\mathbf{5}^{ox}$. Isosbestic points appear at 335 and 442 nm. No evidence of an intermediate oxidation state was observed. UV−vis SEC studies of **1**, **2**, **3a**, and **4** show similar behavior at anodic potentials (Figures S100, S102−S104), with the disappearance of the strong visible transition and the appearance of a new band at 380−420 nm for the oxidized species. The evolution of the UV−vis SEC spectra of **1** in fluorobenzene is nearly identical to the data in acetonitrile, again showing no evidence of an intermediate species (Figure S101).

Computational Studies. DFT calculations were performed to gain a better understanding of the electronic structure of these complexes. Complex **3a** was selected for the initial evaluation of different functionals since the bulky ureayl groups may affect the optimized geometry.[58] Ground-state geometry optimizations of **3a** as a closed-shell singlet using pure or hybrid functionals were able to reproduce key structural metrics with negligible differences between the DFT-calculated and X-ray structures (Tables S26 and S27); however, not all functionals accurately predict the potential inversion (Table S33). From comparing the calculated results with the full set of spectroscopic and electrochemical data for **3a**, we find that the BP86 functional with TZVPP (for Co) and TZVP (for other atoms) basis set shows reliable results, including the calculated second electron transfer being easier than the first (vide infra).

We also considered the antiferromagnetically coupled Co^{II}(low-spin)-(s-bqdi) singlet biradical as a possible electronic structure for **3a**, which would be consistent with the diamagnetism of the neutral complexes. Accessing the antiferromagnetically coupled state using the broken-symmetry (BS) approach failed with BP86 and other pure functionals, instead optimizing to a closed-shell singlet. Similar results have been reported for BS calculations with related complexes, which may be attributed to overestimation of the stability of

https://doi.org/10.1021/acs.inorgchem.3c01283
Inorg. Chem. 2023, 62, 10397−10407

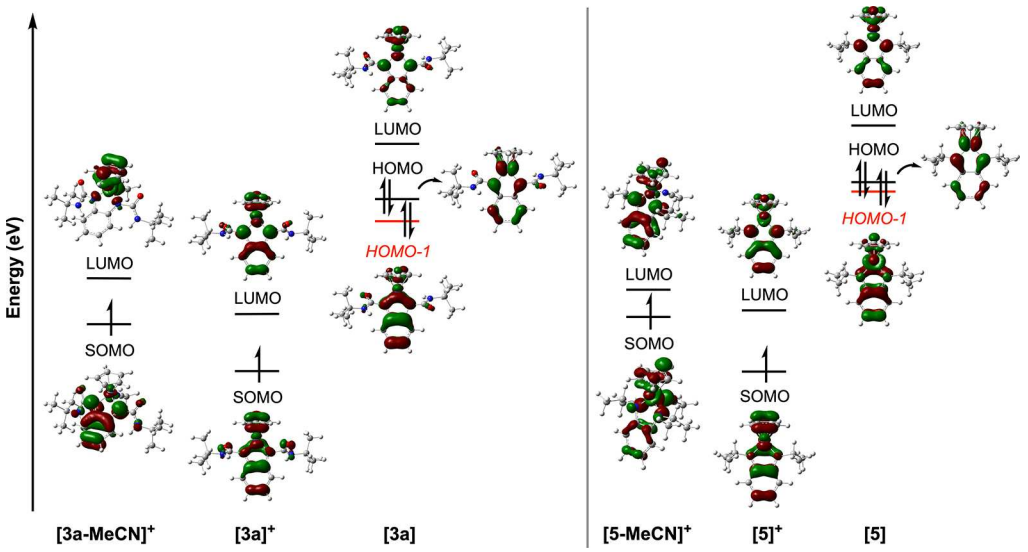

Figure 4. Calculated frontier molecular orbitals (isovalue = 0.04) for **3a**, **5**, and their 1e$^-$ oxidized species.

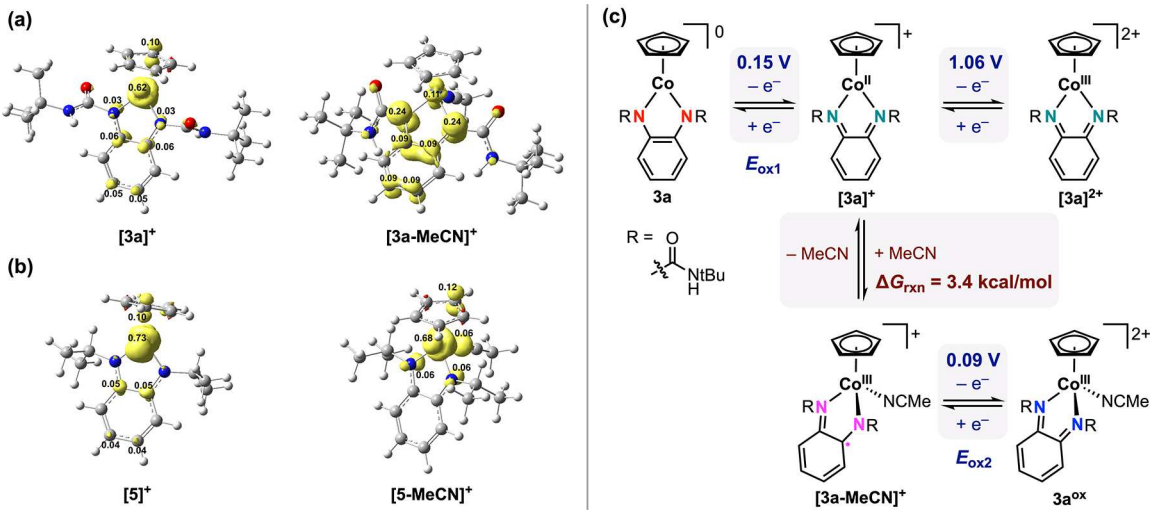

Figure 5. (a) Mulliken spin density plots (isovalue = 0.005) of [**3a**]$^+$ and [**3a-MeCN**]$^+$. (b) Mulliken spin density plots (isovalue = 0.005) of [**5**]$^+$ and [**5-MeCN**]$^+$. (c) Calculated thermodynamic parameters for electron transfer and acetonitrile coordination for **3a**. Potentials in V vs $[Cp_2Fe]^{+/0}$.

spin-paired states by pure functionals.[59] The BS state of **3a** using hybrid functionals was successfully computed, having unpaired spin density located on both cobalt and the phenylenediamide ligand (Figure S107). While slightly lower in energy (−1.4 kcal/mol) than the spin-paired singlet using the B3LYP functional, the optimized structure of the singlet diradical is less consistent with the experimental crystal structure. Moreover, B3LYP fails to predict the 2e$^-$ potential inversion from either the antiferromagnetically coupled diradical or the closed shell singlet, which contradicts our experimental data (Table S33). Overall, the BP86 functional is better able to capture the electronic structure of **3a** compared to the hybrid functionals, and thus the closed shell singlet description for the neutral cobalt complexes was used for all further calculations.

Using our computational approach, we find close agreement between the X-ray structure and calculated geometry for the neutral complexes and isolated oxidized species (Tables S28–S30). Importantly, the increase in the Co−N bond lengths and decrease in the N−$C_{phenylene}$ bond lengths upon 2e$^-$ oxidation are effectively reproduced in the calculated structures, as is the loss of aromaticity in the phenylene ring. Additionally, our DFT calculations predict that the trans geometry of **5** is slightly lower in energy (ca. 1 kcal/mol) compared to the two possible syn geometries (Figure S106).

The calculated HOMO of each neutral complex is the π^*-antibonding combination of the cobalt d_{xy} and ligand π orbitals, which is typical for late transition-metal centers with strong π-donor ligands such as amides (Figures 4 and S115–S119). The HOMO−1 is the π-bonding combination of the cobalt d_{yz} and ligand π^* orbitals, highlighting the covalent nature of this interaction. Together, our results indicate a coordinatively unsaturated, diamagnetic ground-state description for the neutral cobalt complexes, with delocalized bonding and stabilization across the Co−opda metallocycle thanks to effective overlap and mixing between the metal d orbitals and the electron-rich π-system of the opda ligand.

Two-Electron Oxidation Pathway. The calculated potential for the first 1e$^-$ oxidation (E_{ox1}) of **1**–**5** is in excellent agreement with the experimental value for the 2e$^-$ CV feature (Table S33). With each system, loss of one electron yields a monocationic complex in which the calculated spin

https://doi.org/10.1021/acs.inorgchem.3c01283
Inorg. Chem. 2023, 62, 10397−10407

density is mainly on cobalt (low-spin, S_{total} = 1/2; Figures 5a,b and S108−S114). We note that [**2**]$^+$, which contains the Cp* ligand instead of the Cp ligand, has appreciable spin density on both the metal and ligand due to the greater electron-donating character of the Cp* ligand. The 1e$^-$ oxidation of **1**−**5** is accompanied by elongation of the Co−N bonds and shortening of the N−$C_{phenylene}$ bonds, of which the latter indicates an increase in the N−$C_{phenylene}$ bond order upon 1e$^-$ oxidation (Tables S31 and S32). There are also systematic changes to the phenylene backbone, showing a greater degree of C−C bond length alternation and thus a greater loss of aromaticity compared to the neutral complexes. Additionally, there is a noticeable change in the dihedral angle between the Cp ligand and the N−Co−N plane (9−13°). These structural changes indicate that 1e$^-$ oxidation of **1**−**5** leads to a decrease in electron density at the ligand (i.e., an increase in the ligand oxidation state), resulting in structures that resemble the diimine bqdi description. Thus, this intermediate state may be viewed as [$Cp^{R'}Co^{II}(^{R}$bqdi)]$^+$, formed via ligand oxidation and redox-induced electron transfer to cobalt.[60−62]

There are obvious similarities between the HOMO−1 of the neutral complexes and the singly occupied molecular orbital (SOMO) of the monocationic state [**Co**]$^+$ (Figures 4 and S115−S119). In both cases, the orbital is the (cobalt d_{yz})−(ligand π^*) bonding combination. Partial occupation of this π-bonding orbital as the SOMO in [**Co**]$^+$ contributes to weaker metal−ligand bonding and coordination geometry distortions away from the ideal two-legged piano stool structure. In the [**Co**]$^+$ state, we also note that the calculated β-HOMO is at the same or slightly higher energy than the α-SOMO. Such partial inversion of the SOMO and HOMO energies in radical species may occur when conformational changes accompany a redox process, leading to an associated reordering of the frontier orbitals.[63]

Following 1e$^-$ oxidation, coordination of an acetonitrile ligand is energetically accessible (Figure 5c and Table S35). Similar equilibria have been proposed for other [$CpCo^{II}$] systems.[64,65] The first electron loss weakens the cobalt−ligand bonding interactions and decreases the metallocycle aromaticity, as evidenced by the calculated DFT structures. These factors lead to distortion of the two-legged piano stool geometry and prime the cobalt for additional ligand coordination. From here, the loss of the second electron is facile. For example, E_{ox2} = 0.09 V vs $[Cp_2Fe]^{+/0}$ for [**3a-MeCN**]$^+$, 60 mV more negative than the predicted E_{ox1} value for **3a** (Figure 5c). Thus, the oxidation pathway for these complexes is best described by an ECE mechanism. Indeed, potential inversion by this route is predicted for all complexes except for **3b** (where $E_{ox2} - E_{ox1}$ = 5 mV; see Table S33). The importance of structural reorganization for multielectron redox behavior has been noted.[66,67] For **1**−**5**, the initial ligand-based oxidation and electron transfer to cobalt are key to accessing the second electron transfer at mild potentials by promoting the change in coordination geometry. The possibility of an EEC mechanism was also considered, where two 1e$^-$ events are followed by acetonitrile coordination. However, the second 1e$^-$ oxidation is predicted to occur at a much more positive potential. The resulting high-energy, coordinatively unsaturated species, [$Cp^{R'}Co^{III}(^{R}$bqdi)]$^{2+}$, is preferentially stabilized by acetonitrile coordination (Table S35), offsetting the electrostatic penalty of 2e$^-$ oxidation.

Interestingly, looking at the [CpCo] complexes, the location of the second electron transfer varies with the phenylenediamide substituents. With the electron-withdrawing ^{tBuUrea}opda ligand, coordination of acetonitrile to [**3a**]$^+$ causes the unpaired spin density to shift from Co^{II} to the ligand backbone in [**3a-MeCN**]$^+$ (Figure 5a). Meanwhile, the Co−N and N−$C_{phenylene}$ bond lengths in [**3a-MeCN**]$^+$ increase by ca. 0.05 and 0.02 Å, respectively, with small changes to the phenylene backbone (Table S31). Based on these features, [**3a-MeCN**]$^+$ may be described as a Co^{III}-(s-bqdi) system, and the 1e$^-$ oxidation of [**3a-MeCN**]$^+$ to **3a^{ox}** is ligand-based. Similar behavior is predicted for the other ureayl-substituted systems (Figures S110−S112). Conversely, the calculated spin density for [**1-MeCN**]$^+$ is located on the metal with some spin density on the ligand (Figure S108), while the more electron-rich ^{iPr}opda system [**5-MeCN**]$^+$ is predicted to have the spin density more centered on cobalt (Figures 5b, S113 and S114). This behavior is mirrored in the predicted bond length changes, where the structural changes upon acetonitrile coordination to [**1**]$^+$ and [**5**]$^+$ are negligible (Table S32). Thus, the Co^{II}-bqdi description is maintained in [**5-MeCN**]$^+$, and the 1e$^-$ oxidation of [**5-MeCN**]$^+$ to **5^{ox}** is assigned as metal-based. Similar trends are also seen in SOMO for the [**Co-MeCN**]$^+$ species; in [**3a-MeCN**]$^+$, the SOMO is primarily the ^{tBuUrea}opda π^* orbital, while in [**1-MeCN**]$^+$, it has contributions from the ^{H}opda π^* and cobalt d_{yz} orbitals, and in [**5-MeCN**]$^+$, it is mainly the cobalt d_{yz} orbital (Figure 4).

Comparing our systems to related group 9 complexes, there are key differences in behavior.[36−41] As mentioned above, the iridium and rhodium examples have been assigned as coordinatively unsaturated M^{III} centers that are stabilized by the dianionic opda ligand. In our cobalt series, our results also indicate coordinatively unsaturated Co^{III} center with covalent π bonding in the metallocycle, in line with the delocalized bonding description proposed in an early report by Trogler and co-workers.[68] Better energetic matching between the opda π-system and cobalt d orbitals compared to iridium and rhodium is likely responsible for the greater covalent bonding. The iridium and rhodium complexes exhibit either sequential 1e$^-$ or net 2e$^-$ redox couples depending on the ligand structure. Interestingly, Sarkar and co-workers showed that the 2e$^-$ oxidation of [$Cp^*Ir(^{Ph,H}$opda)] by CV is more reversible in less coordinating solvents, suggesting that coordination of an additional ligand is detrimental for 2e$^-$ behavior. The authors also see evidence of the intermediate monocationic state at faster scan rates and by UV−vis SEC. This behavior is in contrast to our cobalt systems, where no intermediate species in the oxidation are observed and the 2e$^-$ wave is highly reversible in acetonitrile. Sarkar and co-workers found comparable behavior with two rhodium complexes, where treatment with a chemical oxidant leads to a [Rh−MeCN]$^{2+}$ complex in acetonitrile or an unusual dinuclear rhodium species in CH_2Cl_2 using Meerwein's salt. With cobalt, we do not see evidence of such ligand loss and dimerization for chemical oxidation in CH_2Cl_2, but further studies are needed to confirm the structure of the reaction product.

Complexes **1**−**5** represent the first example where the potential of a 2e$^-$ redox process at a first-row transition-metal complex is changed by systematically varying the properties of a redox-active ligand. Furthermore, in this series, greater electron-withdrawing character at the ligand favors two ligand-based oxidations (from the π^* orbital), while greater electron-donating character favors one ligand (π^*) and one metal (d_{yz}) oxidation (Figure 6). We note that **2** does not directly align in this trend due to contributions from the electron-rich Cp*

https://doi.org/10.1021/acs.inorgchem.3c01283
Inorg. Chem. 2023, 62, 10397−10407

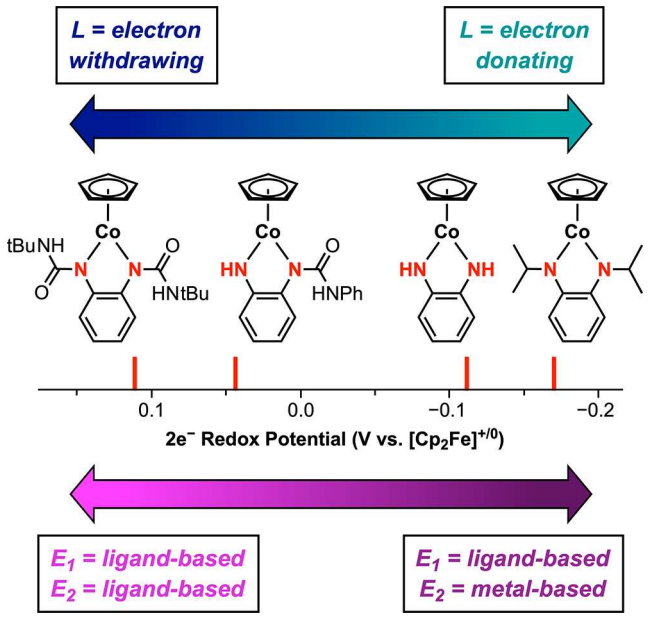

Figure 6. Changes in the sites of 2e⁻ oxidation as a function of the electronic character of the phenylenediamide ligand.

ligand; this system shows significant ligand involvement in the frontier molecular orbitals and spin density for $[\mathbf{2}]^+$ and $[\mathbf{2\text{-}MeCN}]^+$, which is attributed to the greater donating character of Cp* causing greater involvement of the redox-active ligand. Remarkably, despite these differences, all complexes in this study show potential inversion. We attribute this behavior to the effective orbital alignment between cobalt and opda, such that changes to the ligand properties shift the redox potential values but do not disrupt the potential inversion. Our results suggest that further tuning of the ligand properties may access a larger potential range for the 2e⁻ oxidation through redistribution of electron density across the metal d and ligand π^* orbitals. Efforts to establish the limits of this redox tuning and the consequences for reactivity are currently underway.

CONCLUSIONS

Despite several years of investigations into cobalt−opda complexes, the electronic structure and oxidation behavior of half-sandwich complexes $[Cp^{R'}Co(^{R}opda)]$ have yet to be fully elucidated. In this report, we have investigated several examples in this family and shown that all complexes exhibit a 2e⁻ oxidation regardless of the opda substituents. These complexes have covalent π-delocalization in the cobalt−opda metallocycle from close energetic matching of the cobalt d and ligand π^* orbitals. Following an ECE mechanism, loss of the first electron occurs from the ligand with concomitant electron transfer to cobalt, which disrupts the metallocycle bonding interactions and destabilizes the two-legged piano stool geometry, facilitating structural reorganization. Coordination of an acetonitrile ligand in the chemical step preferentially stabilizes the dicationic state, resulting in potential inversion. The electronic properties of the opda ligand not only influence the 2e⁻ oxidation potential but also control the site of the second electron transfer step. This novel behavior offers new opportunities to tune the redox-active ligand properties to control bond formation at a first-row transition-metal center via cooperative metal−ligand electron storage. In this context, we are currently exploring the reactivity of these cobalt complexes with electrophilic reagents to form other Co−X bonds promoted by the phenylenediamide ligand.

ASSOCIATED CONTENT

Supporting Information

The following files are available free of charge. The Supporting Information is available free of charge at https://pubs.acs.org/doi/10.1021/acs.inorgchem.3c01283.

Experimental procedures, crystallographic details, NMR spectra, cyclic voltammetry studies, electronic absorption spectra, and computational results (PDF)

Cartesian coordinates for DFT calculated structures using BP86/def2-TZVP(P) (ZIP)

Accession Codes

CCDC 2183201−2183205 and 2183207−2183213 contain the supplementary crystallographic data for this paper. These data can be obtained free of charge via www.ccdc.cam.ac.uk/data_request/cif, or by emailing data_request@ccdc.cam.ac.uk, or by contacting The Cambridge Crystallographic Data Centre, 12 Union Road, Cambridge CB2 1EZ, UK; fax: +44 1223 336033.

AUTHOR INFORMATION

Corresponding Author

Kate M. Waldie − *Department of Chemistry and Chemical Biology, Rutgers, The State University of New Jersey, Piscataway, New Jersey 08854, United States;* orcid.org/0000-0001-6444-6122; Email: kate.waldie@rutgers.edu

Authors

Minzhu Zou − *Department of Chemistry and Chemical Biology, Rutgers, The State University of New Jersey, Piscataway, New Jersey 08854, United States;* orcid.org/0000-0002-2710-135X

Thomas J. Emge − *Department of Chemistry and Chemical Biology, Rutgers, The State University of New Jersey, Piscataway, New Jersey 08854, United States*

Complete contact information is available at: https://pubs.acs.org/10.1021/acs.inorgchem.3c01283

Author Contributions

Conceptualization, M.Z. and K.M.W.; methodology, M.Z. and K.M.W.; investigation, M.Z. and T.J.E.; writing − original draft, M.Z. and K.M.W.; writing − review and editing, M.Z. and K.M.W.; supervision, K.M.W.

Notes

The authors declare no competing financial interest.

A previous version of this manuscript was previously deposited as a preprint in ChemRxiv.[69]

ACKNOWLEDGMENTS

This work was supported by the ACS Petroleum Research Fund (65171-DNI3) and Rutgers, The State University of New Jersey. The Rigaku SYNERGY-S X-ray diffractometer was partially funded by an NSF MRI Award (CHE-2117792) to the Rutgers University Department of Chemistry and Chemical Biology. We acknowledge the Office of Advanced Research Computing (OARC) at Rutgers University for providing access to the Amarel Cluster and associated research computing resources. We acknowledge Prof. Roger A.

Lalancette (Rutgers University, Newark) for additional X-ray data collection and discussions.

REFERENCES

(1) Zell, T.; Langer, R. From Ruthenium to Iron and Manganese—A Mechanistic View on Challenges and Design Principles of Base-Metal Hydrogenation Catalysts. *ChemCatChem* **2018**, *10* (9), 1930−1940.
(2) Storr, T.; Mukherjee, R. Preface for the Forum on Applications of Metal Complexes with Ligand-Centered Radicals. *Inorg. Chem.* **2018**, *57* (16), 9577−9579.
(3) Evans, D. H. One-Electron and Two-Electron Transfers in Electrochemistry and Homogeneous Solution Reactions. *Chem. Rev.* **2008**, *108* (7), 2113−2144.
(4) Bullock, R. M. Reaction: Earth-Abundant Metal Catalysts for Energy Conversions. *Chem* **2017**, *2* (4), 444−446.
(5) Ludwig, J. R.; Schindler, C. S. Catalyst: Sustainable Catalysis. *Chem* **2017**, *2* (3), 313−316.
(6) Arevalo, R.; Chirik, P. J. Enabling Two-Electron Pathways with Iron and Cobalt: From Ligand Design to Catalytic Applications. *J. Am. Chem. Soc.* **2019**, *141* (23), 9106−9123.
(7) Bullock, R. M.; Chen, J. G.; Gagliardi, L.; Chirik, P. J.; Farha, O. K.; Hendon, C. H.; Jones, C. W.; Keith, J. A.; Klosin, J.; Minteer, S. D.; Morris, R. H.; Radosevich, A. T.; Rauchfuss, T. B.; Strotman, N. A.; Vojvodic, A.; Ward, T. R.; Yang, J. Y.; Surendranath, Y. Using nature's blueprint to expand catalysis with Earth-abundant metals. *Science* **2020**, *369* (6505), No. eabc3183.
(8) Chirik, P. J.; Wieghardt, K. Radical Ligands Confer Nobility on Base-Metal Catalysts. *Science* **2010**, *327* (5967), 794−795.
(9) Chirik, P. J. Preface: Forum on Redox-Active Ligands. *Inorg. Chem.* **2011**, *50* (20), 9737−9740.
(10) Kaim, W. Manifestations of Noninnocent Ligand Behavior. *Inorg. Chem.* **2011**, *50* (20), 9752−9765.
(11) van der Vlugt, J. I. Radical-Type Reactivity and Catalysis by Single-Electron Transfer to or from Redox-Active Ligands. *Chem.—Eur. J.* **2019**, *25* (11), 2651−2662.
(12) van Leest, N. P.; de Zwart, F. J.; Zhou, M.; de Bruin, B. Controlling Radical-Type Single-Electron Elementary Steps in Catalysis with Redox-Active Ligands and Substrates. *JACS Au* **2021**, *1* (8), 1101−1115.
(13) Richert, S. A.; Tsang, P. K. S.; Sawyer, D. T. Ligand-centered redox processes for manganese, iron and cobalt, MnL_3, FeL_3, and CoL_3, complexes (L = acetylacetonate, 8-quinolinate, picolinate, 2,2'-bipyridyl, 1,10-phenanthroline) and for their tetrakis(2,6-dichlorophenyl)porphinato complexes[M(Por)]. *Inorg. Chem.* **1989**, *28* (12), 2471−2475.
(14) Bartlett, P. N.; Eastwick-Field, V. A reinvestigation of the electrochemistry of $[Ni(II)(bpy)_3(ClO_4))_2]$ in acetonitrile using rotating disc and rotating ring-disc electrodes. *Electrochim. Acta* **1993**, *38* (17), 2515−2523.
(15) Ghosh, P.; Samanta, S.; Roy, S. K.; Joy, S.; Krämer, T.; McGrady, J. E.; Goswami, S. Redox Noninnocence in Coordinated 2-(Arylazo)pyridines: Steric Control of Ligand-Based Redox Processes in Cobalt Complexes. *Inorg. Chem.* **2013**, *52* (24), 14040−14049.
(16) Sengupta, D.; Ghosh, P.; Chatterjee, T.; Datta, H.; Paul, N. D.; Goswami, S. Ligand-Centered Redox in Nickel(II) Complexes of 2-(Arylazo)pyridine and Isolation of 2-Pyridyl-Substituted Triaryl Hydrazines via Catalytic N-Arylation of Azo-Function. *Inorg. Chem.* **2014**, *53* (22), 12002−12013.
(17) Sampson, M. D.; Nguyen, A. D.; Grice, K. A.; Moore, C. E.; Rheingold, A. L.; Kubiak, C. P. Manganese Catalysts with Bulky Bipyridine Ligands for the Electrocatalytic Reduction of Carbon Dioxide: Eliminating Dimerization and Altering Catalysis. *J. Am. Chem. Soc.* **2014**, *136* (14), 5460−5471.
(18) Waldie, K. M.; Ramakrishnan, S.; Kim, S.-K.; Maclaren, J. K.; Chidsey, C. E. D.; Waymouth, R. M. Multielectron Transfer at Cobalt: Influence of the Phenylazopyridine Ligand. *J. Am. Chem. Soc.* **2017**, *139* (12), 4540−4550.
(19) Matson, B. D.; McLoughlin, E. A.; Armstrong, K. C.; Waymouth, R. M.; Sarangi, R. Effect of Redox Active Ligands on the Electrochemical Properties of Manganese Tricarbonyl Complexes. *Inorg. Chem.* **2019**, *58* (11), 7453−7465.
(20) Richburg, C. S.; Farnum, B. H. Influence of Pyridine on the Multielectron Redox Cycle of Nickel Diethyldithiocarbamate. *Inorg. Chem.* **2019**, *58* (22), 15371−15384.
(21) Mazumder, M. M. R.; Burton, A.; Richburg, C. S.; Saha, S.; Cronin, B.; Duin, E.; Farnum, B. H. Controlling One-Electron vs Two-Electron Pathways in the Multi-Electron Redox Cycle of Nickel Diethyldithiocarbamate. *Inorg. Chem.* **2021**, *60* (17), 13388−13399.
(22) Bamberger, H.; Albold, U.; Dubnická Midlíková, J.; Su, C.-Y.; Deibel, N.; Hunger, D.; Hallmen, P. P.; Neugebauer, P.; Beerhues, J.; Demeshko, S.; Meyer, F.; Sarkar, B.; van Slageren, J. Iron(II), Cobalt(II), and Nickel(II) Complexes of Bis(sulfonamido)benzenes: Redox Properties, Large Zero-Field Splittings, and Single-Ion Magnets. *Inorg. Chem.* **2021**, *60* (5), 2953−2963.
(23) Sharma, S. K.; May, P. S.; Jones, M. B.; Lense, S.; Hardcastle, K. I.; MacBeth, C. E. Catalytic dioxygen activation by Co(II) complexes employing a coordinatively versatile ligand scaffold. *Chem. Commun.* **2011**, *47* (6), 1827−1829.
(24) Chlopek, K.; Bothe, E.; Neese, F.; Weyhermuller, T.; Wieghardt, K. Molecular and Electronic Structures of Tetrahedral Complexes of Nickel and Cobalt Containing *N,N'*-Disubstituted, Bulky *o*-Diiminobenzosemiquinonate(1−) π-Radical Ligands. *Inorg. Chem.* **2006**, *45* (16), 6298−6307.
(25) Chaudhuri, P.; Verani, C. N.; Bill, E.; Bothe, E.; Weyhermüller, T.; Wieghardt, K. Electronic Structure of Bis(*o*-iminobenzosemiquinonato)metal Complexes (Cu, Ni, Pd). The Art of Establishing Physical Oxidation States in Transition-Metal Complexes Containing Radical Ligands. *J. Am. Chem. Soc.* **2001**, *123* (10), 2213−2223.
(26) Bill, E.; Bothe, E.; Chaudhuri, P.; Chlopek, K.; Herebian, D.; Kokatam, S.; Ray, K.; Weyhermüller, T.; Neese, F.; Wieghardt, K. Molecular and Electronic Structure of Four- and Five-Coordinate Cobalt Complexes Containing Two *o*-Phenylenediamine- or Two *o*-Aminophenol-Type Ligands at Various Oxidation Levels: An Experimental, Density Functional, and Correlated ab initio Study. *Chem.—Eur. J.* **2005**, *11* (1), 204−224.
(27) Herebian, D.; Bothe, E.; Neese, F.; Weyhermüller, T.; Wieghardt, K. Molecular and Electronic Structures of Bis-(*o*-diiminobenzosemiquinonato)metal(II) Complexes (Ni, Pd, Pt), Their Monocations and -Anions, and of Dimeric Dications Containing Weak Metal−Metal Bonds. *J. Am. Chem. Soc.* **2003**, *125* (30), 9116−9128.
(28) Ray, K.; Petrenko, T.; Wieghardt, K.; Neese, F. Joint spectroscopic and theoretical investigations of transition metal complexes involving non-innocent ligands. *Dalton Trans.* **2007**, No. 16, 1552−1566.
(29) Broere, D. L. J.; Plessius, R.; van der Vlugt, J. I. New avenues for ligand-mediated processes − expanding metal reactivity by the use of redox-active catechol, *o*-aminophenol and *o*-phenylenediamine ligands. *Chem. Soc. Rev.* **2015**, *44* (19), 6886−6915.
(30) Skara, G.; Gimferrer, M.; De Proft, F.; Salvador, P.; Pinter, B. Scrutinizing the Noninnocence of Quinone Ligands in Ruthenium Complexes: Insights from Structural, Electronic, Energy, and Effective Oxidation State Analyses. *Inorg. Chem.* **2016**, *55* (5), 2185−2199.
(31) Rajput, A.; Sharma, A. K.; Barman, S. K.; Saha, A.; Mukherjee, R. Valence tautomerism and delocalization in transition metal complexes of o-amidophenolates and other redox-active ligands. Some recent results. *Coord. Chem. Rev.* **2020**, *414*, 213240.
(32) Koten, G. V.; Vrieze, K. 1,4-Diaza-1,3-butadiene (α-Diimine) Ligands: Their Coordination Modes and the Reactivity of Their Metal Complexes. *Adv. Organomet. Chem.* **1982**, *21*, 151−239.
(33) Greulich, S.; Kaim, W.; Stange, A. F.; Stoll, H.; Fiedler, J.; Záliš, S. Cp*Ir(dab) (dab =1,4-Bis(2,6-dimethylphenyl)-1,4-diazabutadiene): A Coordinatively Unsaturated Six-π-Electron Metallaheteroaromatic Compound? *Inorg. Chem.* **1996**, *35* (13), 3998−4002.
(34) Smith, A. L.; Hardcastle, K. I.; Soper, J. D. Redox-Active Ligand-Mediated Oxidative Addition and Reductive Elimination at

https://doi.org/10.1021/acs.inorgchem.3c01283
Inorg. Chem. 2023, 62, 10397−10407

Square Planar Cobalt(III): Multielectron Reactions for Cross-Coupling. *J. Am. Chem. Soc.* **2010**, *132* (41), 14358−14360.
(35) van der Meer, M.; Rechkemmer, Y.; Peremykin, I.; Hohloch, S.; van Slageren, J.; Sarkar, B. (Electro)catalytic C−C bond formation reaction with a redox-active cobalt complex. *Chem. Commun.* **2014**, *50* (76), 11104−11106.
(36) Ringenberg, M. R.; Kokatam, S. L.; Heiden, Z. M.; Rauchfuss, T. B. Redox-Switched Oxidation of Dihydrogen Using a Non-Innocent Ligand. *J. Am. Chem. Soc.* **2008**, *130* (3), 788−789.
(37) van der Meer, M.; Manck, S.; Sobottka, S.; Plebst, S.; Sarkar, B. Redox Activity and Bond Activation in Iridium−Diamidobenzene Complexes: A Combined Structural, (Spectro)electrochemical, and DFT Investigation. *Organometallics* **2015**, *34* (22), 5393−5400.
(38) Sobottka, S.; van der Meer, M. B.; Glais, E.; Albold, U.; Suhr, S.; Su, C.-Y.; Sarkar, B. A coordinatively unsaturated iridium complex with an unsymmetrical redox-active ligand: (spectro)electrochemical and reactivity studies. *Dalton Trans.* **2019**, *48* (37), 13931−13942.
(39) Suhr, S.; Walter, R.; Beerhues, J.; Albold, U.; Sarkar, B. Rhodium diamidobenzene complexes: a tale of different substituents on the diamidobenzene ligand. *Chem. Sci.* **2022**, *13* (35), 10532−10545.
(40) Blacker, A. J.; Clot, E.; Duckett, S. B.; Eisenstein, O.; Grace, J.; Nova, A.; Perutz, R. N.; Taylor, D. J.; Whitwood, A. C. Synthesis and structure of "16-electron" rhodium(III) catalysts for transfer hydrogenation of a cyclic imine: mechanistic implications. *Chem. Commun.* **2009**, No. 44, 6801−6803.
(41) Fujita, D.; Kaga, A.; Sugimoto, H.; Morimoto, Y.; Itoh, S. Controlling Coordination Number of Rhodium(III) Complex by Ligand-Based Redox for Catalytic C−H Amination. *Bull. Chem. Soc. Jpn.* **2020**, *93* (2), 279−286.
(42) Rheingold, A. L.; Fultz, W. C.; Brill, T. B.; Landon, S. J. Crystal and molecular structure of (η^5-C_5H_5)Co(HNC_6H_4NH), a cobalt *o*-quinonediimine complex. *J. Crystallogr. Spectrosc. Res.* **1983**, *13* (5), 317−323.
(43) Miller, E. J.; Brill, T. B. The metal atom's view of the bonding in *o*-benzoquinone, *o*-dithiobenzoquinone, and *o*-benzoquinone diimine metallacycles of cyclopentadienylcobalt. A cobalt-59 NQR study of the *cis*-a_3b_2 ligand geometry. *Inorg. Chem.* **1983**, *22* (17), 2392−2398.
(44) Miller, E. J.; Rheingold, A. L.; Brill, T. B. Bonding and structure in cyclopentadienylcobaltmetallacycle complexes. The crystal structures of [η^5-$C_5(CH_3)_5$]Co[$(NH)_2C_6H_4$] and [η^5-$C_5(CH_3)_5$]Co-[$(NH)SC_6H_4$]. *J. Organomet. Chem.* **1985**, *282* (3), 399−412.
(45) Reinhardt, M.; Dalgleish, S.; Shuku, Y.; Reissig, L.; Matsushita, M. M.; Crain, J.; Awaga, K.; Robertson, N. Molecular and thin film properties of cobalt half-sandwich compounds for optoelectronic application. *Phys. Chem. Chem. Phys.* **2017**, *19* (9), 6768−6776.
(46) Pilia, L.; Shuku, Y.; Dalgleish, S.; Hofmann, D. W. M.; Melis, N.; Awaga, K.; Robertson, N. Effect of fluorination on the crystal and electronic structure of organometallic cyclopentadienyl-phenylenediamino-cobalt complexes. *J. Organomet. Chem.* **2020**, *918*, 121277.
(47) Štrukil, V.; Margetić, D.; Igrc, M. D.; Eckert-Maksić, M.; Friščić, T. Desymmetrisation of aromatic diamines and synthesis of non-symmetrical thiourea derivatives by click-mechanochemistry. *Chem. Commun.* **2012**, *48* (78), 9705−9707.
(48) Ould, D. M. C.; Rigby, A. C.; Wilkins, L. C.; Adams, S. J.; Platts, J. A.; Pope, S. J. A.; Richards, E.; Melen, R. L. Investigations into the Photophysical and Electronic Properties of Pnictoles and Their Pnictenium Counterparts. *Organometallics* **2018**, *37* (5), 712−719.
(49) Rajabimoghadam, K.; Darwish, Y.; Bashir, U.; Pitman, D.; Eichelberger, S.; Siegler, M. A.; Swart, M.; Garcia-Bosch, I. Catalytic Aerobic Oxidation of Alcohols by Copper Complexes Bearing Redox-Active Ligands with Tunable H-Bonding Groups. *J. Am. Chem. Soc.* **2018**, *140* (48), 16625−16634.
(50) Heck, R. F. Cyclopentadienylcobalt Derivatives of Chelating Aromatic Ligands. *Inorg. Chem.* **1968**, *7* (8), 1513−1516.
(51) Miller, E. J.; Landon, S. J.; Brill, T. B. Pentamethylcyclopentadienyl (.eta.5-$C_5(CH_3)_5$) vs. cyclopentadienyl (.eta.5-C_5H_5). A comparison of electronic influences for metallocenes with *fac*-a_3b_2c, *fac*-a_3b_3, and *cis*-a_3b_2 ligand geometry based on cobalt-59 NQR spectroscopy. *Organometallics* **1985**, *4* (3), 533−538.
(52) Connelly, N. G.; Geiger, W. E. Chemical Redox Agents for Organometallic Chemistry. *Chem. Rev.* **1996**, *96* (2), 877−910.
(53) Metcalfe, R. A.; Lever, A. B. P. Tetraammineruthenium(II) and -ruthenium(III) Complexes of *o*-Benzoquinone Diimine and Their Redox Series. *Inorg. Chem.* **1997**, *36* (21), 4762−4771.
(54) Bugarcic, T.; Habtemariam, A.; Deeth, R. J.; Fabbiani, F. P. A.; Parsons, S.; Sadler, P. J. Ruthenium(II) Arene Anticancer Complexes with Redox-Active Diamine Ligands. *Inorg. Chem.* **2009**, *48* (19), 9444−9453.
(55) Bard, A. J.; Faulkner, L. R., Electrode Reactions with Coupled Homogeneous Chemical Reactions. In *Electrochemical Methods: Fundamentals and Applications*, 2nd ed.; John Wiley & Sons, Inc.: New York, NY, 2001; pp 471−533.
(56) Smith, A. L.; Clapp, L. A.; Hardcastle, K. I.; Soper, J. D. Redox-active ligand-mediated Co−Cl bond-forming reactions at reducing square planar cobalt(III) centers. *Polyhedron* **2010**, *29* (1), 164−169.
(57) Barrière, F.; Geiger, W. E. Use of Weakly Coordinating Anions to Develop an Integrated Approach to the Tuning of $\Delta E_{1/2}$ Values by Medium Effects. *J. Am. Chem. Soc.* **2006**, *128* (12), 3980−3989.
(58) Minkin, V. I.; Starikov, A. G.; Starikova, A. A. Computational insight into magnetic behavior and properties of the transition metal complexes with redox-active ligands: a DFT approach. *Pure Appl. Chem.* **2018**, *90* (5), 811−824.
(59) Herebian, D.; Wieghardt, K. E.; Neese, F. Analysis and Interpretation of Metal-Radical Coupling in a Series of Square Planar Nickel Complexes: Correlated Ab Initio and Density Functional Investigation of [$Ni(L^{ISQ})_2$] (L^{ISQ} = 3,5-di-*tert*-butyl-*o*-diiminobenzosemiquinonate(1-)). *J. Am. Chem. Soc.* **2003**, *125* (36), 10997−11005.
(60) Miller, J. S.; Min, K. S. Oxidation Leading to Reduction: Redox-Induced Electron Transfer (RIET). *Angew. Chem., Int. Ed.* **2009**, *48* (2), 262−272.
(61) Piskunov, A. V.; Pashanova, K. I.; Bogomyakov, A. S.; Smolyaninov, I. V.; Starikov, A. G.; Fukin, G. K. Cobalt complexes with hemilabile *o*-iminobenzoquinonate ligands: a novel example of redox-induced electron transfer. *Dalton Trans.* **2018**, *47* (42), 15049−15060.
(62) Lohmeyer, L.; Schön, F.; Kaifer, E.; Himmel, H.-J. Stimulation of Redox-Induced Electron Transfer by Interligand Hydrogen Bonding in a Cobalt Complex with Redox-Active Guanidine Ligand. *Angew. Chem., Int. Ed.* **2021**, *60* (18), 10415−10422.
(63) Talipov, M. R.; Boddeda, A.; Lindeman, S. V.; Rathore, R. Does Koopmans' Paradigm for 1-Electron Oxidation Always Hold? Breakdown of IP/E_{ox} Relationship for *p*-Hydroquinone Ethers and the Role of Methoxy Group Rotation. *J. Phys. Chem. Lett.* **2015**, *6* (17), 3373−3378.
(64) Elgrishi, N.; Kurtz, D. A.; Dempsey, J. L. Reaction Parameters Influencing Cobalt Hydride Formation Kinetics: Implications for Benchmarking H_2-Evolution Catalysts. *J. Am. Chem. Soc.* **2017**, *139* (1), 239−244.
(65) Kurtz, D. A.; Dhar, D.; Elgrishi, N.; Kandemir, B.; McWilliams, S. F.; Howland, W. C.; Chen, C.-H.; Dempsey, J. L. Redox-Induced Structural Reorganization Dictates Kinetics of Cobalt(III) Hydride Formation via Proton-Coupled Electron Transfer. *J. Am. Chem. Soc.* **2021**, *143* (9), 3393−3406.
(66) Macías-Ruvalcaba, N. A.; Evans, D. H. Electron Transfer and Structural Change: Distinguishing Concerted and Two-Step Processes. *Chem.—Eur. J.* **2007**, *13* (16), 4386−4395.
(67) Fortage, J.; Peltier, C.; Perruchot, C.; Takemoto, Y.; Teki, Y.; Bedioui, F.; Marvaud, V.; Dupeyre, G.; Pospísil, L.; Adamo, C.; Hromadová, M.; Ciofini, I.; Lainé, P. P. Single-Step versus Stepwise Two-Electron Reduction of Polyarylpyridiniums: Insights from the Steric Switching of Redox Potential Compression. *J. Am. Chem. Soc.* **2012**, *134* (5), 2691−2705.
(68) Gross, M. E.; Ibers, J. A.; Trogler, W. C. Structural and spectroscopic study of cyclopentadienylcobalt (*N*-phenyl-*o*-benzoqui-

https://doi.org/10.1021/acs.inorgchem.3c01283
Inorg. Chem. 2023, 62, 10397−10407

none diimines). A case for delocalized π bonding. *Organometallics* **1982**, *1* (3), 530−535.
(69) Zou, M.; Emge, T. J.; Waldie, K. M. Two-Electron Redox Tuning of Cyclopentadienyl Cobalt Complexes Enabled by the Phenylenediamide Ligand. *ChemRxiv* **2023**, DOI: 10.26434/chemrxiv-2023-l58hm.

https://doi.org/10.1021/acs.inorgchem.3c01283
Inorg. Chem. 2023, 62, 10397−10407